

ON-LINE APPENDIX: METHODS

Devices

All image processing was performed on a Mac Pro 2.7 GHz Quad-Core Intel Xeon E5 desktop computer (MacIntosh, with 32 GB 1867 MHz DDR3 memory running OS X 10.9.5; Microsoft, Bothell, Washington). FSL, Version 5.0.7, and Matlab R2014a v8.3.0.532 were used for all image processing.

Image Acquisition

Imaging data were obtained on either a 1.5T or 3T TwinSpeed Excite scanner (GE Healthcare, Milwaukee, Wisconsin) or a 1.5T or 3T Achieva (Philips Healthcare, Best, the Netherlands) MR imaging scanner. Voxel sizes for each cohort were as follows:

Cohort 1. DWI: $0.429 \times 0.429 \times 5$ ($n = 10$) or $0.859 \times 0.859 \times 5$ ($n = 14$)

FLAIR: $0.491 \times 0.491 \times 5$ ($n = 6$), $0.859 \times 0.859 \times 5$ ($n = 16$), or $0.937 \times 0.937 \times 5$ ($n = 2$)

T1WI: $0.392 \times 0.392 \times 5$ ($n = 6$), $0.429 \times 0.429 \times 5$ ($n = 4$), $0.572 \times 0.572 \times 5$ ($n = 9$), or $0.859 \times 0.859 \times 5$ ($n = 5$).

Cohort 2. DWI: $0.429 \times 0.429 \times 5$ ($n = 2$), $0.859 \times 0.859 \times 5$ ($n = 6$); FLAIR: $0.859 \times 0.859 \times 5$ ($n = 6$), $1.145 \times 1.145 \times 5.2$ ($n = 2$)

T1WI: $0.572 \times 0.572 \times 5$ ($n = 2$), $0.687 \times 0.687 \times 5$ ($n = 2$), or $0.859 \times 0.859 \times 5$ ($n = 4$).

Image-Processing Routines

The full image processing pipeline is outlined here with average processing times given per patient.

Image Reconstruction and File Organization (34 Seconds). Matlab was used to read the header information from every DICOM file to ensure that the patient medical record number, scan date, and MR imaging sequence matched the file naming and structure.

Image conversion from DICOM to anonymized NIFTI format was performed by using the `dcm2nii` utility developed by Chris Rorden (<http://www.nitrc.org/projects/mricron/>).

Brain Extraction (268 Seconds for Automated Extraction). `flirt -in <low_res_image> -ref <MNI152lin_T1_2 mm standard> -out <output_image> -omat <initial_matrix> -bins 256 -cost corratio -searchrx 0 0 -searchry 0 0 -searchrz 0 0 -dof nine -interp trilinear`

`convert_xfm -omat <inverse_matrix> -inverse <initial_matrix>`

`flirt -in <MNI_space_brain_mask> -applyxfm -init <inverse_matrix> -out <low_res_mask> -padding 0.0 -interp trilinear -ref <low_res_image>`

`fslmaths <low_res_mask> -bin <low_res_mask>`

`fslmaths <low_res_image> -mul <low_res_mask> <preliminary_brain>`

`bet <preliminary_brain> <preliminary_brain> -f <f-value> -g <g-value> -c 256 256 16 fslview <preliminary_brain> <low_res_mask>`.

Brain extraction ends with a command to call `fslview` and manually review each extraction. Matlab can be made to accept user input to either accept the registration or rerun the registration after adjusting extraction options (eg, `f` value and `g` value), or

the brain extraction can be manually corrected. A nonacceptable automated extraction will increase the processing time. Once `f` and `g` values were chosen for a given imaging sequence, reregistration with different parameters was not common (<10% of brain extractions); instead, we erred toward manually editing brain extractions, which was almost always due to poor extraction in the region of the middle cranial fossa on the T1-weighted images. In total, 60% of brain extractions required no adjustment, with the remainder requiring some amount of editing or repeat extraction with new parameters. Manual editing requires between 1 and 8 minutes, depending on the quality of brain extraction and image resolution. Therefore, if it was applied to future datasets, we would allocate up to 3 minutes of added processing time per brain to be analyzed.

Registration and Generation of Temporal Subtraction Maps (2100 Seconds). `flirt -in <prior_brain> -ref <recurrent_brain> -out <prior2recurrent_brain> -omat <prior2recurrent_brain.mat> -bins 256 -cost mutualinfo -searchrx 0 0 -searchry 0 0 -searchrz 0 0 -dof nine -interp trilinear`

`flirt -in <prior_brain> -ref <recurrent_brain> -out <prior2recurrent_brain> -omat <prior2recurrent_brain.mat> -bins 256 -cost mutualinfo -searchrx 0 0 -searchry 0 0 -searchrz 0 0 -dof nine -interp trilinear`

`flirt -in <prior_brain> -ref <T1_recurrence_brain> -out <prior2T1> -omat <prior2T1.mat> -bins 256 -cost corratio -searchrx 0 0 -searchry 0 0 -searchrz 0 0 -dof nine -interp trilinear`
`convert_xfm -omat <T12prior.mat> -inverse <prior2T1.mat>`

`flirt -in <tumor_mask> -applyxfm -init <T12prior.mat> -out <prior_brain_tumor_mask> -padding 0.0 -interp trilinear -ref <prior_brain>`

`fslmaths <prior_brain_tumor_mask> -thr 0.4 -bin <prior_brain_tumor_mask>`

`*fast -t <image_type> -n three -H 0.1 -I four -l 20.0 -g -o <segmented_brain> <input_brain>`.

`Z` score images were generated (“`z_score_brain`”) in the native scan space in Matlab by performing a voxelwise conversion of the image-intensity values by using the “normal brain” mean and SD computed outside the “`tumor_mask`” volume (see “Materials and Methods” in the text).

`flirt -in <z_score_brain> -applyxfm -init <prior2T1.mat> -out <z_score_hires_brain> -padding 0.0 -interp trilinear -ref <T1_recurrence_brain>`.

After temporal subtraction maps were made and the regression model was run for all patients in cohort 1, the “`mvregress`” function in Matlab was used to compute the parameter estimates to find the least-squares fit of the `z` score images from T1WI, ADC, and FLAIR images to the radiology-defined masks. The parameter estimates were then multiplied by the corresponding imaging sequences from cohort 2. This process requires <10 seconds of computing time:

`prior_brain`: the brain extracted scan that was last read without disease progression
`recurrent_brain`: the brain extracted scan that first showed nodular recurrence

`tumor_mask`: all tumor with a 1.50 to 2-cm margin, per radiation target volume contouring guidelines (see “Materials and Methods” in the text).

Optional Tissue Segmentation Subtraction maps can be generated only for tissue compartments of interest, depending on the research question. For example, tissue segmentation can be performed (eg, with the FMRIB Automated Segmentation Tool in FSL; <http://fsl.fmrib.ox.ac.uk/fsl/fslwiki/FAST>), and the CSF compartment can be excluded from the subtraction images so that only the gray and white matter will be analyzed. In the above example, “image_type” refers to the MR imaging sequence (eg, T1 or T2), “segmented_brain” is the output from FAST with each tissue compartment segmented as a separate image, and “input_brain” is the image to be segmented. Subtraction maps can be generated only for the compartment of interest, which usually excludes the CSF. This process adds approximately 4 minutes to the processing time and did not change the results of the present data measurably, so we consider it an optional step. Note that tissue segmentation should be checked manually for accuracy.

Registration Accuracy

To assess the accuracy of the image registration used to generate the temporal subtraction maps, we applied the 48 coregistration matrices generated in FSL to anatomically defined contours of the brain gray matter. Tissue segmentation was performed by using the FAST toolbox in FSL to generate a binary gray matter mask.

Tissue segmentation into CSF, white matter and gray matter compartments was performed in the native space for all T1WI, ADC, and FLAIR sequences performed at the time of disease recurrence (“recurrent scan”) and on the scan before recurrence (“prior scan”). The transformation matrix generated in the subtraction map registration was applied to the prior scan to register it to the recurrent scan. Accuracy was quantified by calculating the “target overlap” as defined in Klein et al,²⁰ in which 14 image-registration algorithms were compared and placed into 3 categories: rank 1 (high accuracy), rank 2 (intermediate accuracy), and rank 3 (poor accuracy). Target overlap (*TO*), a measure of registration agreement, is the intersection of the source (*S*) volume and target (*T*) volume divided by the target volume:

$$TO = \frac{|S \cap T|}{|T|}$$

Target overlap calculations for the 48 registrations performed in the current study demonstrated a high accuracy across nearly every registration performed. *TO* means (SDs) for T1WI, ADC, and FLAIR registrations were 0.763 (0.1), 0.647 (0.12), 0.695 (0.185), respectively. These results are presented graphically in On-line Fig 2. It is difficult to apply cutoffs for registration accuracy by using the methods of Klein et al²⁰ to our data because that study assessed accuracy among different brains, whereas our study assessed only intrasubject registration accuracy. Applying the approach of Klein et al adds some objective context to our registration accuracy assessment, but without strict cutoffs for accuracy, our results are somewhat subjective. Our post hoc assessment of registration accuracy revealed mean *TO*s that suggest high accuracy. Therefore, nonlinear registration was not used to minimize processing time. However, future work can consider other registration algorithms, including nonlinear registration or linear registration with other software packages, to potentially improve results.

ON-LINE RESULTS

Patient B experienced a small focal recurrence (0.22 mL) in the left internal capsule (On-line Fig 5A, -B). The regression model prediction for the area at high risk for disease (On-line Fig 5C) was covered entirely by the GKRS prescription isodose line (On-line Fig 5D), and no significant clusters were visible outside this region. At 248 days post-GKRS, the lesion remained well-controlled (On-line Fig 5E) and T1WI (On-line Fig 5F, red arrow), but there was early evidence of multifocal disease progression outside the GKRS treatment field in the left anterior frontal lobe (green arrow). At 323 days post-GKRS, the treated lesion remained stable by size criteria, but there was significant multifocal progression in the left anterior frontal lobe. Unthresholded axial images are also provided for patient B in On-line Fig 6.

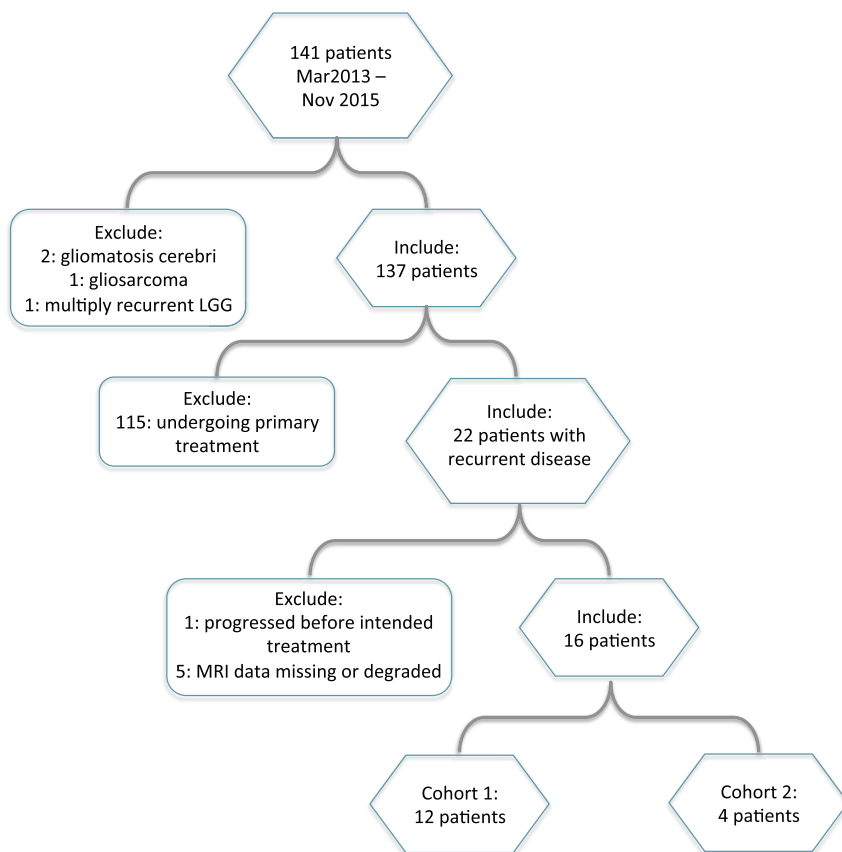
Patient C was found to have a focal recurrence (1.02 mL) in the right inferior temporal lobe (On-line Fig 7A, -B), and the model predicted a high likelihood of recurrence in this area (On-line Fig 7C). The area was covered by the GKRS prescription isodose line (On-line Fig 7D) and demonstrated likely posttreatment changes at 95 days (On-line Fig 7E, -F) and 137 days (On-line Fig 7G, -H). As in patient A, the primary site of disease more superiorly was also evaluated at the same time points. Adjacent to the area, at the right side of the genu of the corpus callosum, there was a region of increased FLAIR intensity and T1WI contrast enhancement (On-line Fig 8A, -B). This was confirmed by application of the model showing areas at high likelihood for tumor recurrence (On-line Fig 8C). For confirmation, this area was outside the right inferior temporal lobe GKRS treatment field (On-line Fig 8D). The superior lesion is presented at 53 days (On-line Fig 8E, -F) and 95 days (On-line Fig 8G, -H) and demonstrates disease progression across the corpus callosum, consistent with the prediction of the model. Unthresholded axial images are also provided for patient C in On-line Fig 9.

Patient D was found to have a focus of nodular recurrence (3.45 mL) in the left medial frontal lobe (On-line Fig 10A, -B), which was highly correlated with the regression model (On-line Fig 10C). GKRS was administered to the area (On-line Fig 10D), and the lesion remained stable at 64-day follow-up imaging (On-line Fig 10E, -F), but it was seen to progress by 134 days (On-line Fig 10G, -H). Also in patient D, voxels within the primary bifrontal lesion (On-line Fig 11A, -B) were highly correlated with the model (On-line Fig 11C). However, unlike the primary lesion observed in patients A and C, these areas were covered by the GKRS treatment isodose line (On-line Fig 11D) and were stable at 64 days (On-line Fig 11E, -F). The area did eventually show signs of progression by 134 days (On-line Fig 11G, -H). Unthresholded axial images are also provided for patient D in On-line Fig 12.

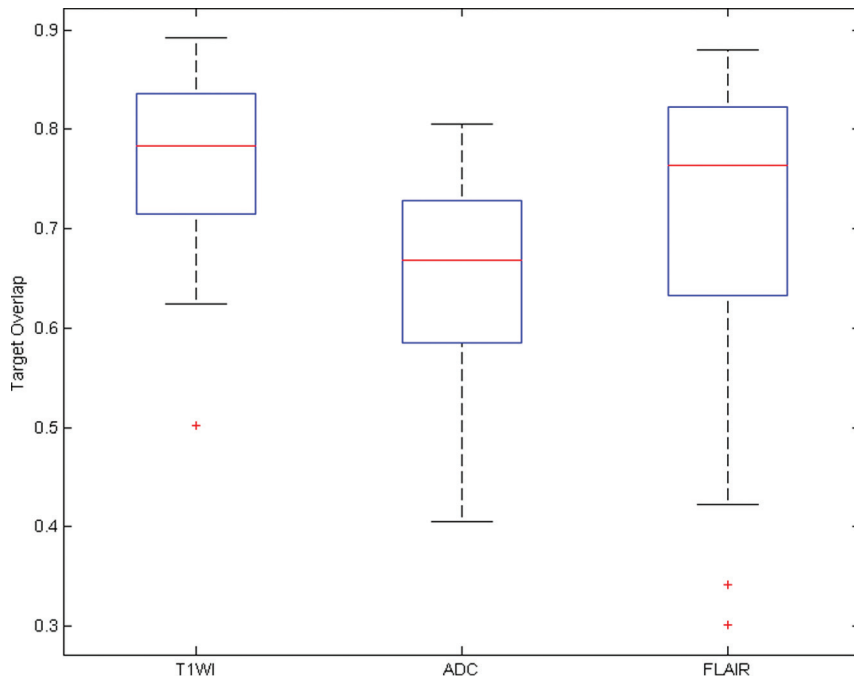
To demonstrate the results of temporal subtraction maps in the posttreatment setting, the results of the analysis performed on patient D by using interval imaging after GKRS are shown in On-line Fig 13A (unthresholded images) and -B (thresholded images). Routine follow-up imaging performed 47 and 76 days postradiosurgery (29-day subtraction interval) was used to generate temporal subtraction maps and demonstrate false-positive voxels within blood vessels, due to a large difference in contrast timing, but there are no dominant findings within the brain parenchyma.

Finally, as mentioned in the “Materials and Methods,” we took a hypothesis-driven approach with assumptions regarding the pattern of change across T1WI, ADC, and FLAIR sequences. To confirm that this did not lead to spurious results, we repeated our full data analysis without any assumptions regarding the pattern of change.

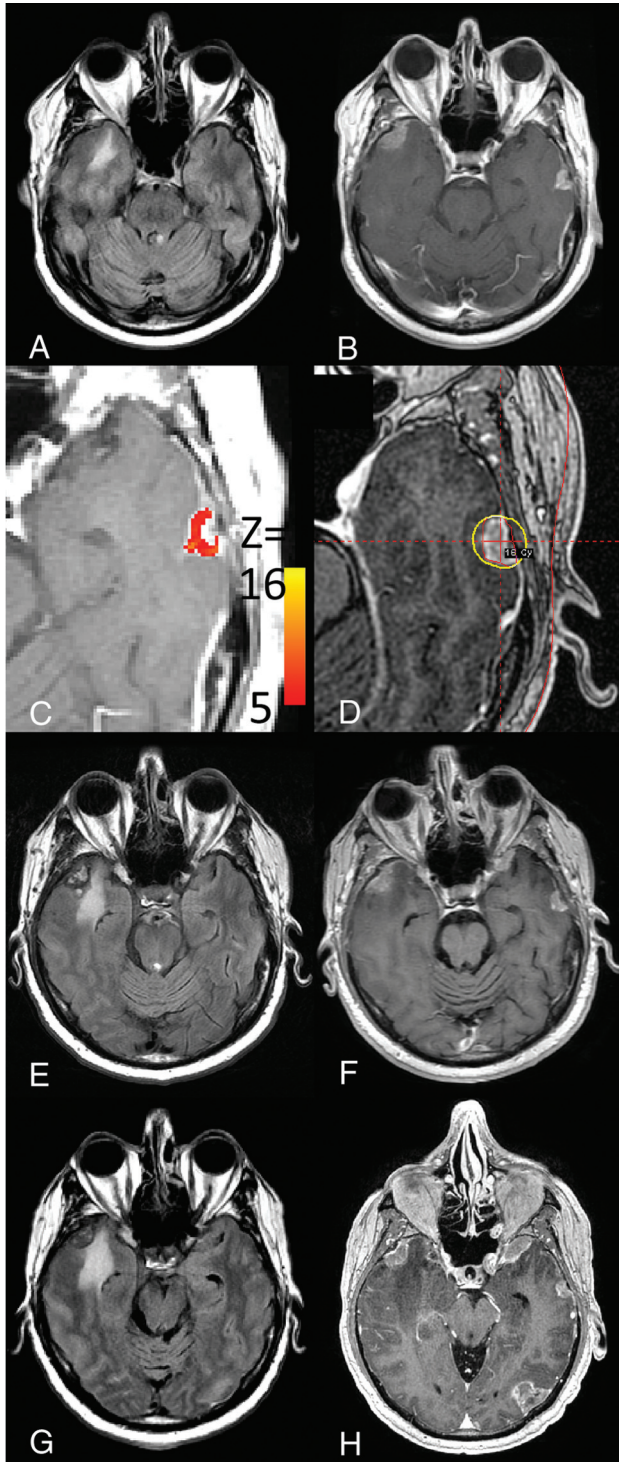
Consistent with the less restricted scope of the regression, more voxels were identified that correlated with the model. Unthresholded axial images are provided in On-line Figs 15–17 for patients A–D, in which the nodular recurrences identified through the hypothesis-driven analysis persist, but with a higher level of background intensity.



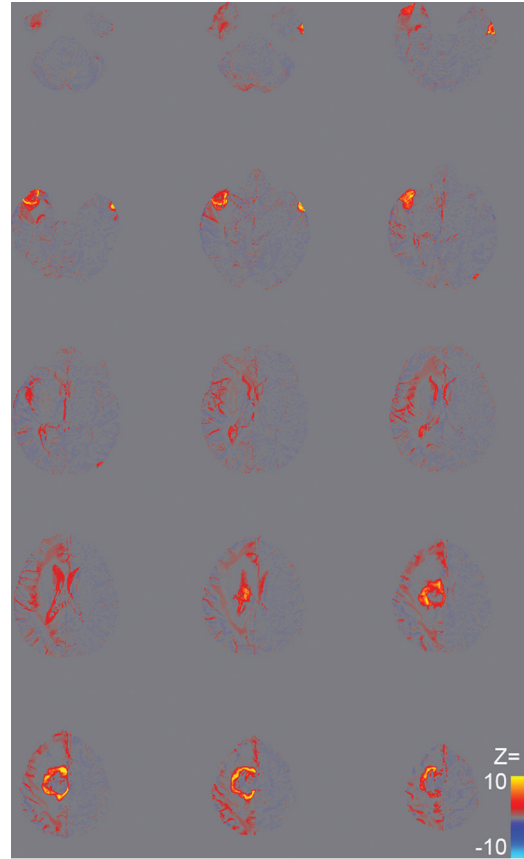
ON-LINE FIG 1. Patient selection to derive 2 cohorts: Twelve patients were treated with external beam radiation (cohort 1), and 4 patients, with radiosurgery (cohort 2). LGG indicates low-grade glioma.



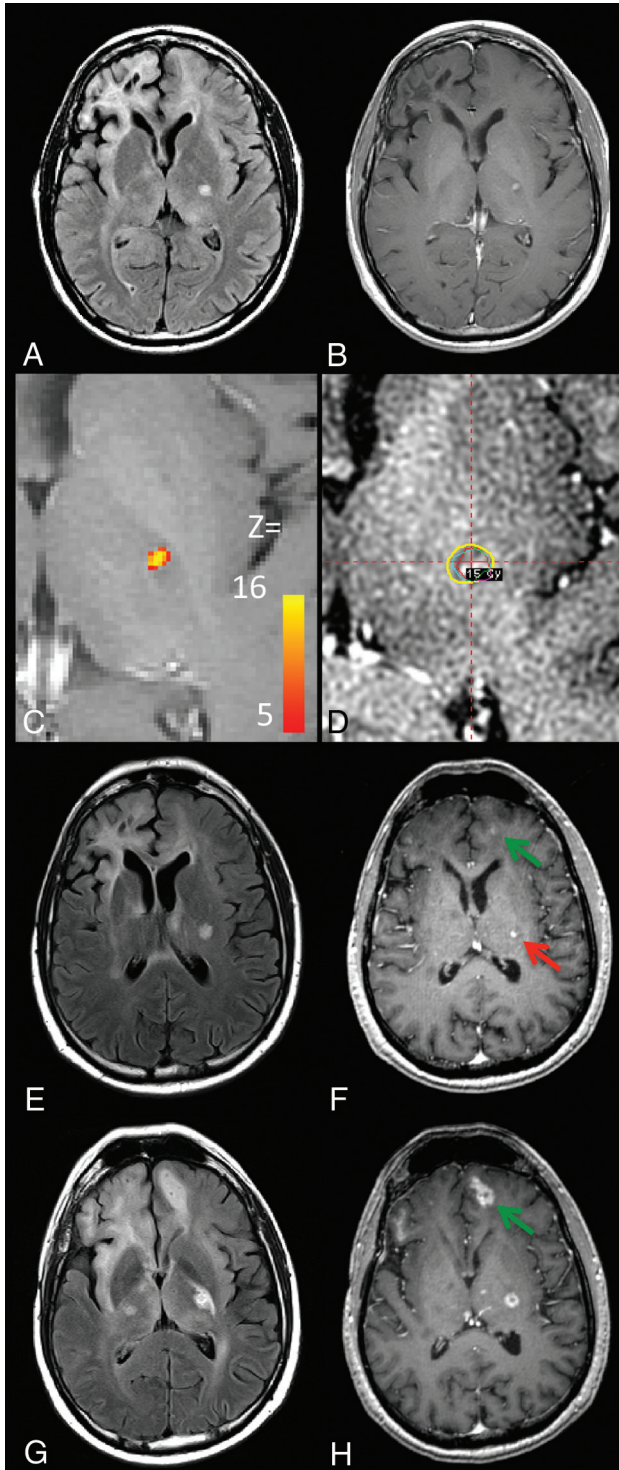
ON-LINE FIG 2. Boxplot demonstrating temporal subtraction map registration accuracy for all imaging sequences across 16 patients included in the study (48 total coregistrations). Gray matter segmentation was performed in the native space of each imaging time point and registered to the scan demonstrating recurrence, to generate a temporal subtraction map. Target overlap of 2 registered ROIs above a value of 0.49 is considered highly accurate.



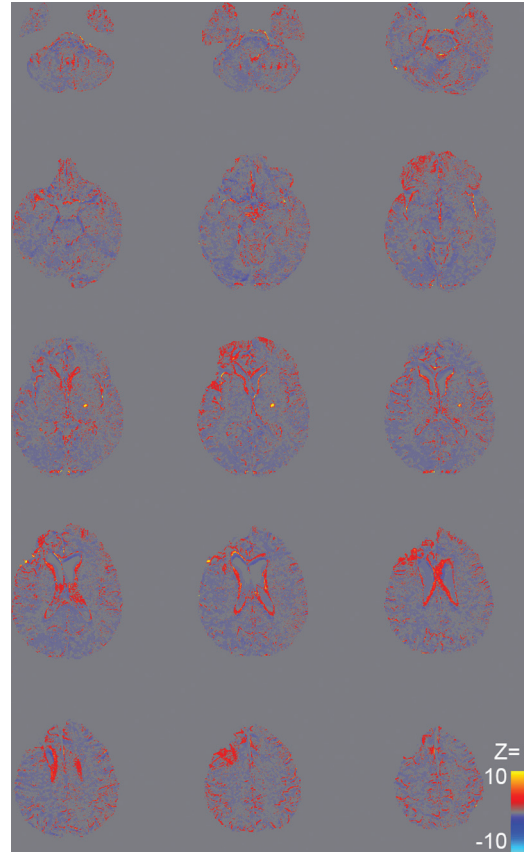
ON-LINE FIG 3. Patient A from the Table was found to have 2 areas of new focal recurrence. The left temporal lesion is depicted here as seen on follow-up imaging (A and B) and determined on the multiparametric subtraction map (C). The area was treated with radiosurgery (D) and was stable at 35 (E and F) and 66 days (G and H), consistent with adequate treatment.



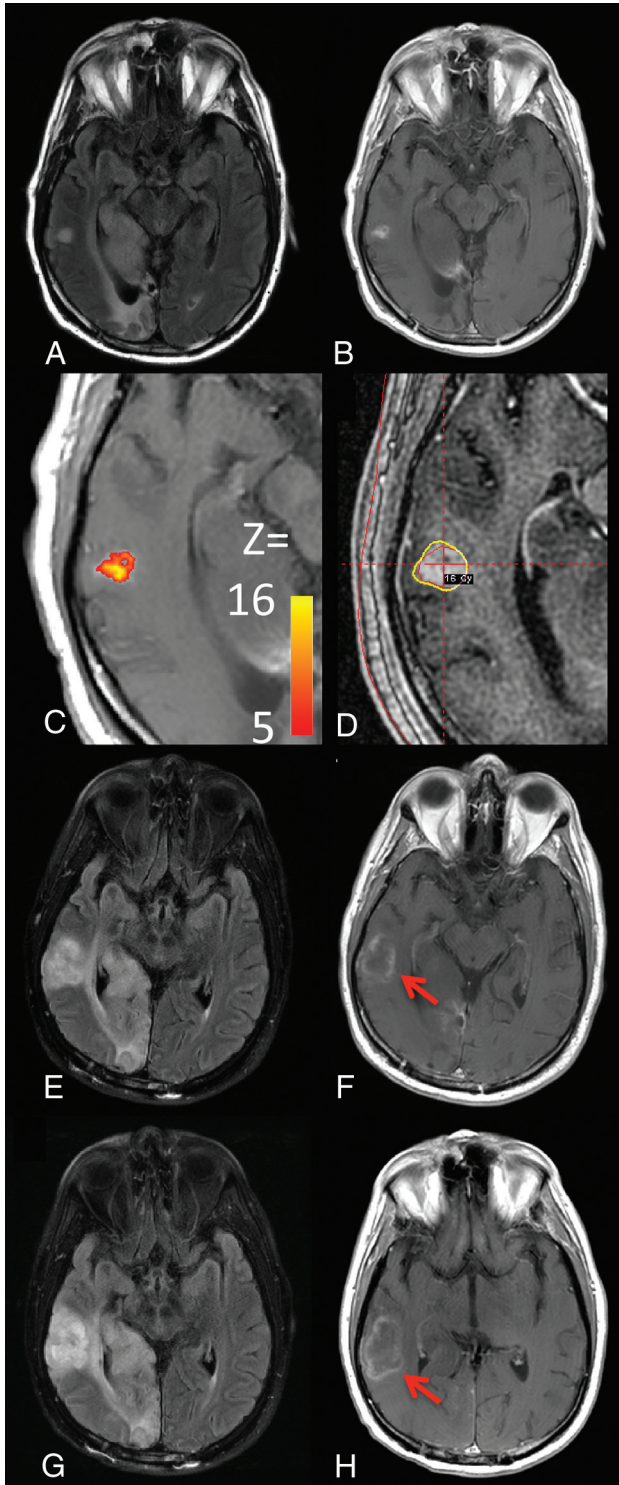
ON-LINE FIG 4. Results from the temporal subtraction map analysis displayed in On-line Fig 3, but without cluster or z statistic thresholds. The color bar is presented for display purposes to demonstrate the range of voxels with a negative (z score ≤ -10 in deep blue), positive (z score ≥ 10 in bright yellow), or no (z score = 0 in gray) correlation to the model.



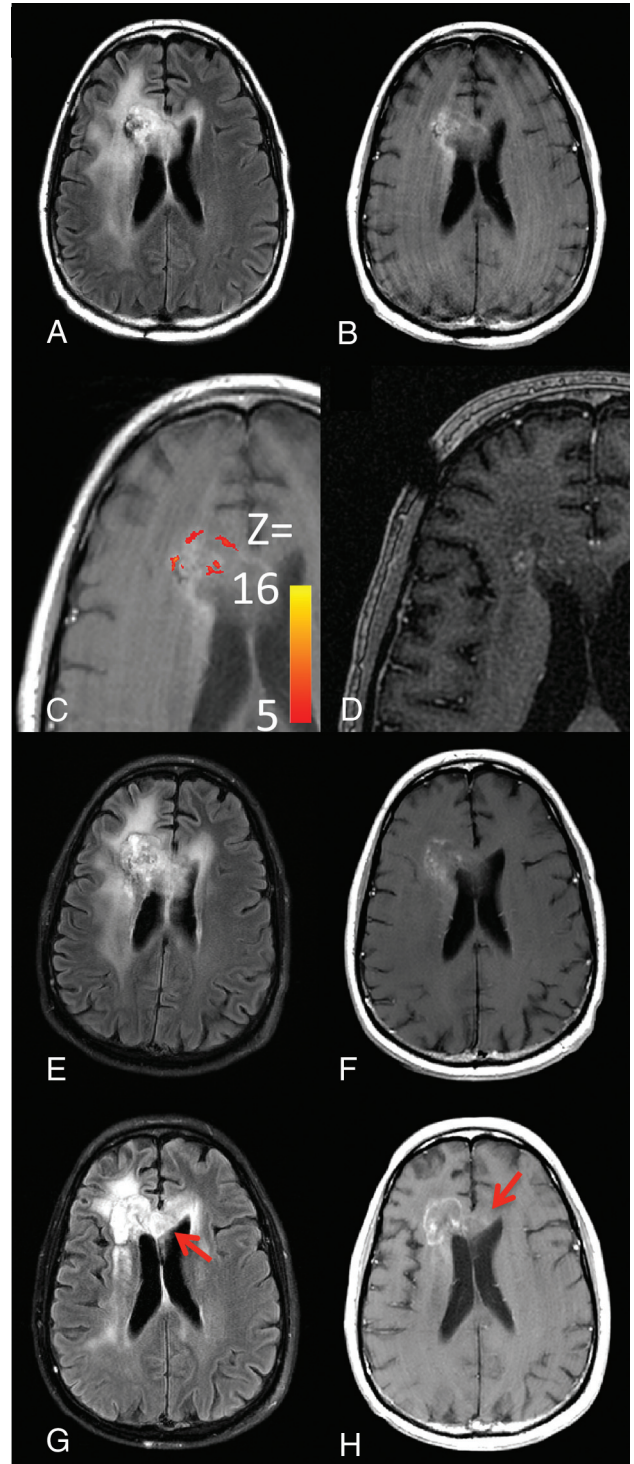
ON-LINE FIG 5. Patient B from the Table experienced a focal nodular recurrence in the left internal capsule (A and B), which could be identified by the multiparametric subtraction map as voxels reaching statistical significance of a z score = 5 (C). This region was treated with radiosurgery (D) and was stable for 248 days on FLAIR (E and F, red arrow), but the condition progressed elsewhere in the brain by 323 days (G and H). Green arrows represent a focus of recurrence that presented at 323 days postradiosurgery but could be seen retrospectively at 248 days.



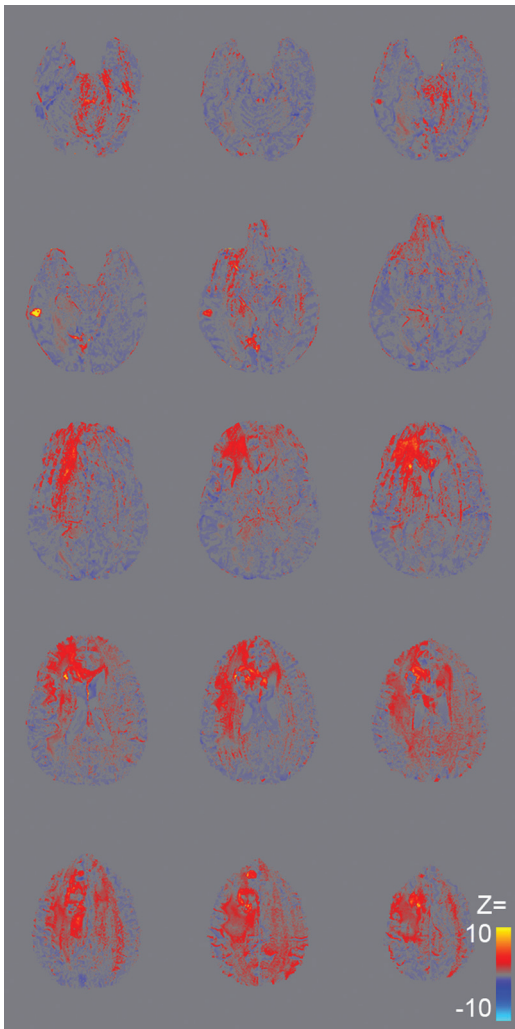
ON-LINE FIG 6. As in On-line Fig 4, unthresholded images are presented for patient B to provide the full range of z scores resulting from the temporal subtraction method.



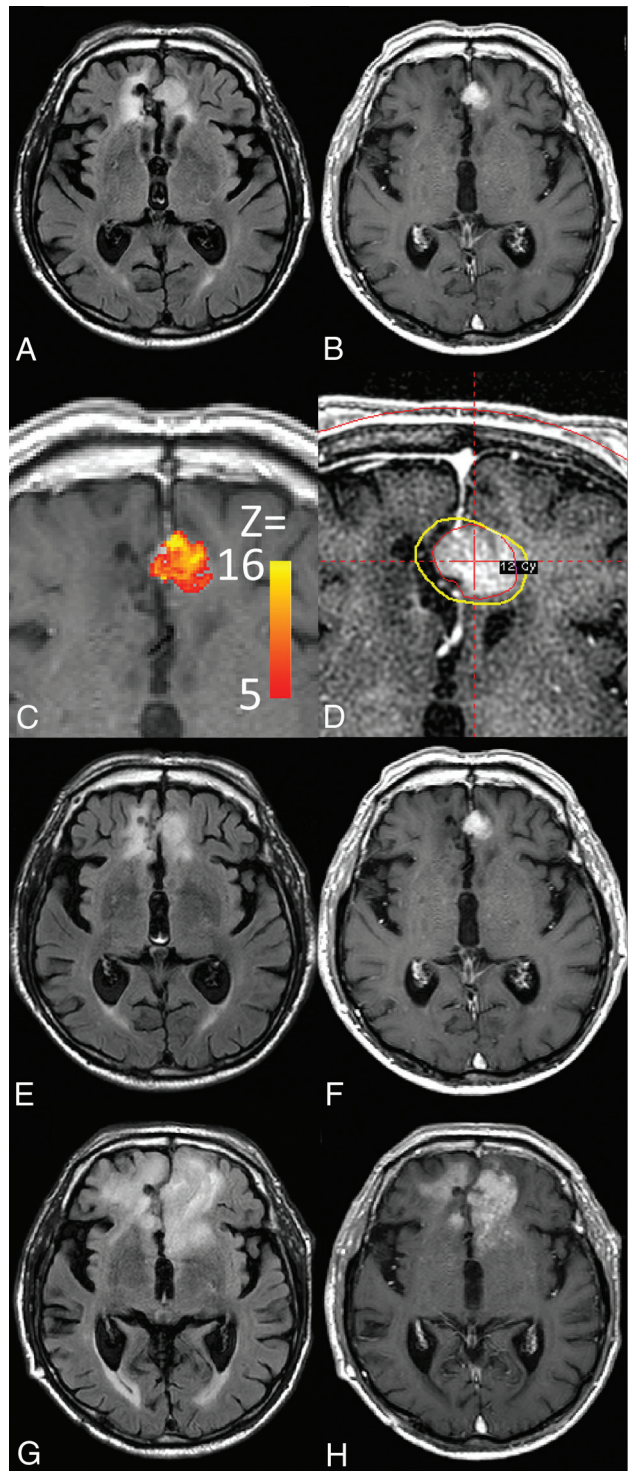
ON-LINE FIG 7. Patient C was found to have a focal recurrence in the right inferior temporal lobe (A and B), which was identified by the regression model (C). Radiosurgery was used to treat the lesion (D), and it was imaged again at 95 (E and F) and 137 days (G and H). Review of radiology reports for each of these time points revealed concern for progression versus pseudoprogression, but this area was thought less likely to represent progression relative to the primary site of disease in the left frontal lobe.



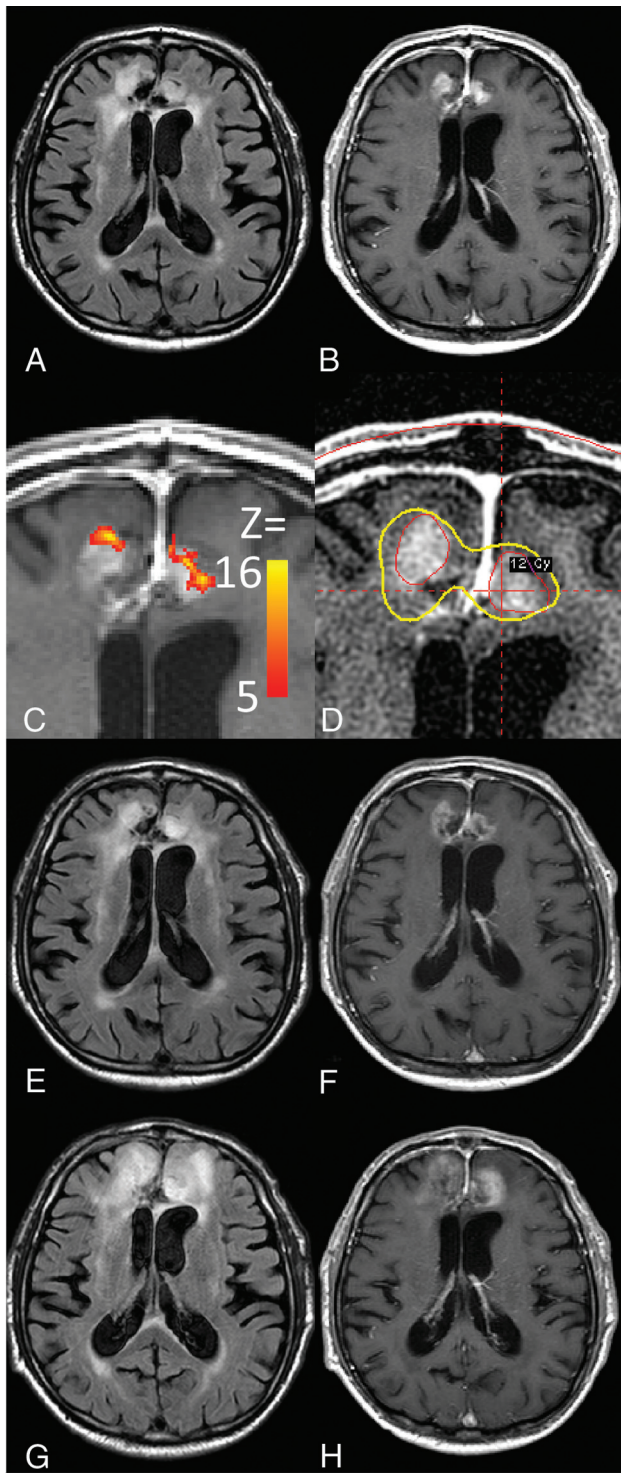
ON-LINE FIG 8. In patient C, the primary site of disease was found to have a region of increased FLAIR intensity and T1WI enhancement (A and B). The regression model identified in this area was seen as having a high likelihood for tumor recurrence (C), but it was not treated with radiosurgery (D) due to its size, unconfirmed progression, and overlap with previous radiation fields. As in On-line Fig 7, the lesion was seen at 53 days (E and F) and 95 days (G and H) and was interpreted as suspicious for disease progression at these time points.



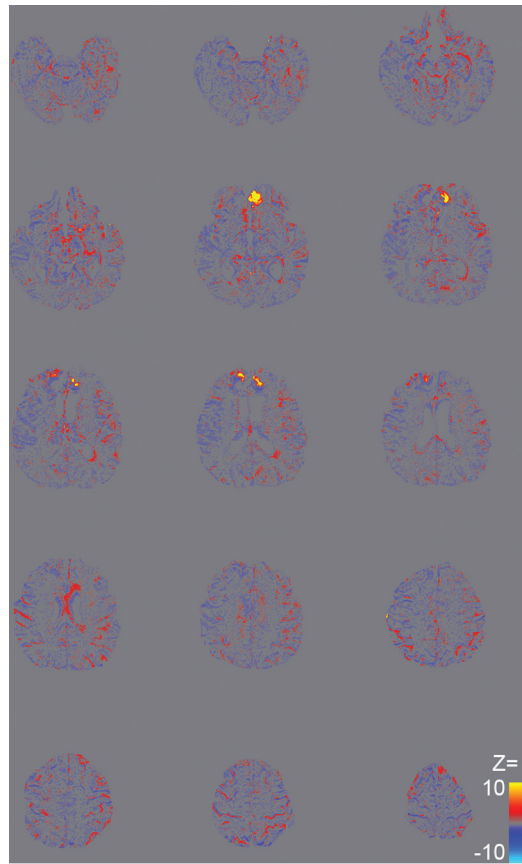
ON-LINE FIG 9. As with the patients presented previously, the full range of z scores is provided in axial images without the application of any statistical thresholds.



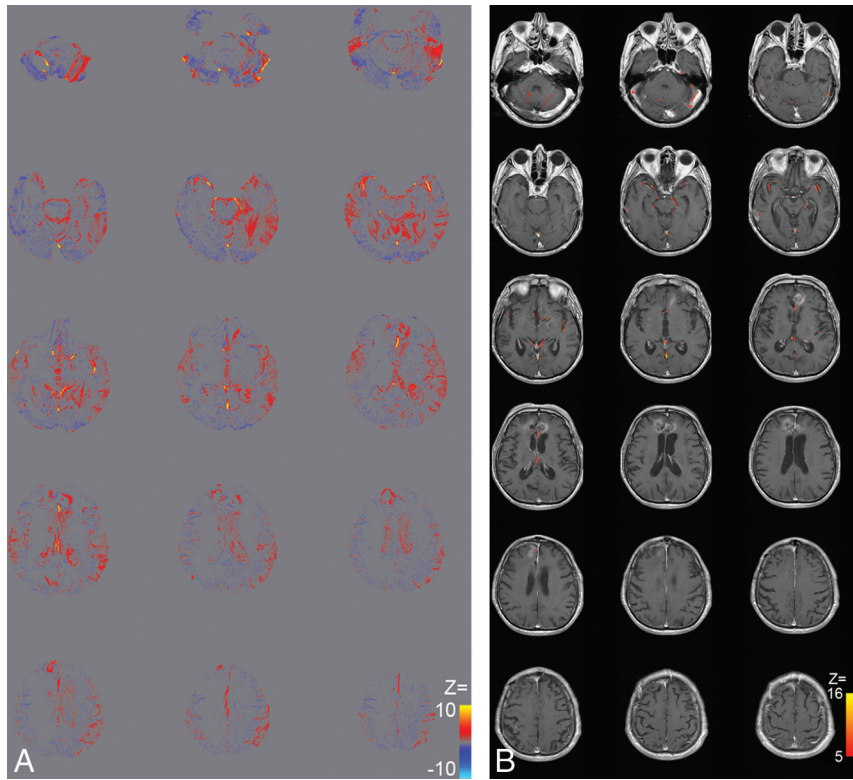
ON-LINE FIG 10. Patient D was found to have a nodular recurrence in the left medial frontal lobe (A and B), which was highly correlated with the regression model (C). Radiosurgery was used to treat to the lesion (D), and it remained stable at 64-day follow-up (E and F). The lesion did eventually progress by 134 days (G and H).



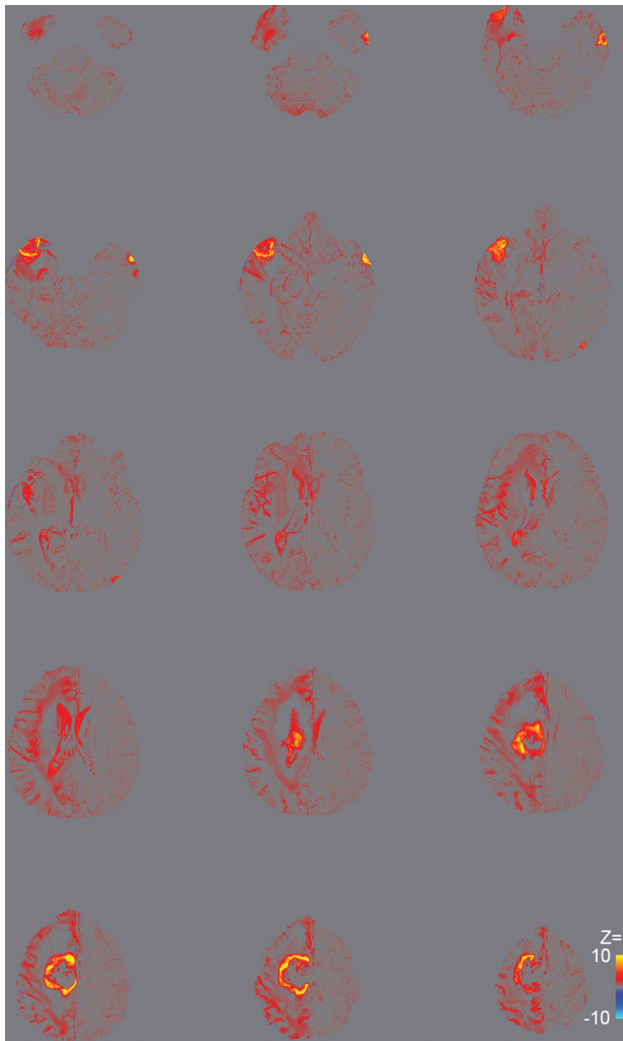
ON-LINE FIG 11. Further evaluation of patient D reveals voxels within the primary bifrontal lesion (A and B), which were identified by the regression model (C). These areas were covered by the radiosurgery treatment isodose line (D), and they were also stable at 64 days (E and F) and progressed by 134 days (G and H).



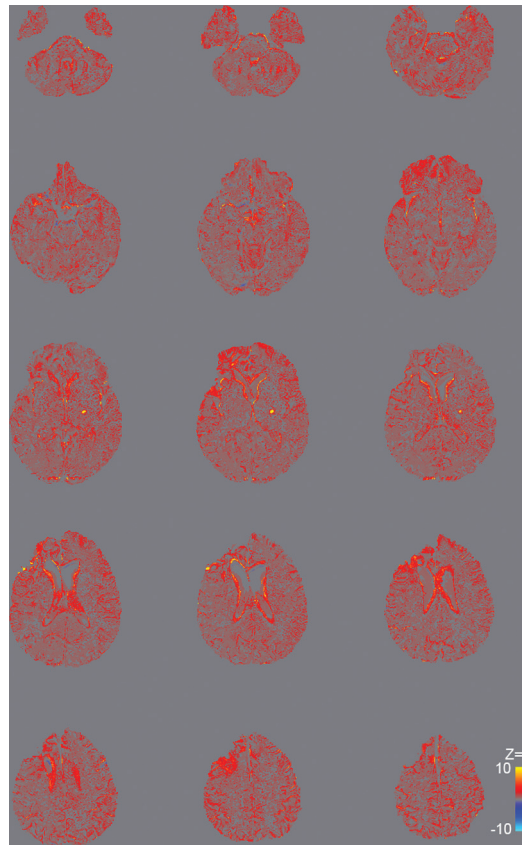
ON-LINE FIG 12. As with patients A–C, the full range of z scores is provided without any thresholds applied.



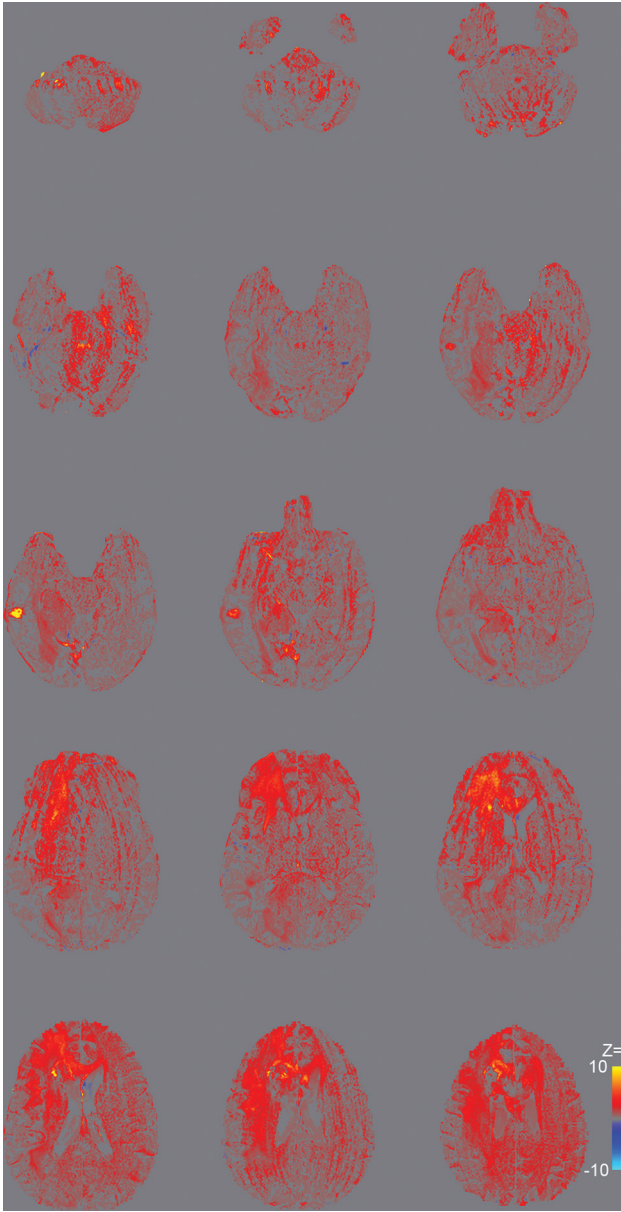
ON-LINE FIG 13. To evaluate the outcome of the subtraction map method in the setting of prior treatment, we analyzed follow-up scans from patient D at 47 and 76 days post-GKRS. Unthresholded (A) axial images demonstrate no dominant lesions in the brain parenchyma, and the only voxels reaching our statistical threshold (B) are at the brain surface and within blood vessels.



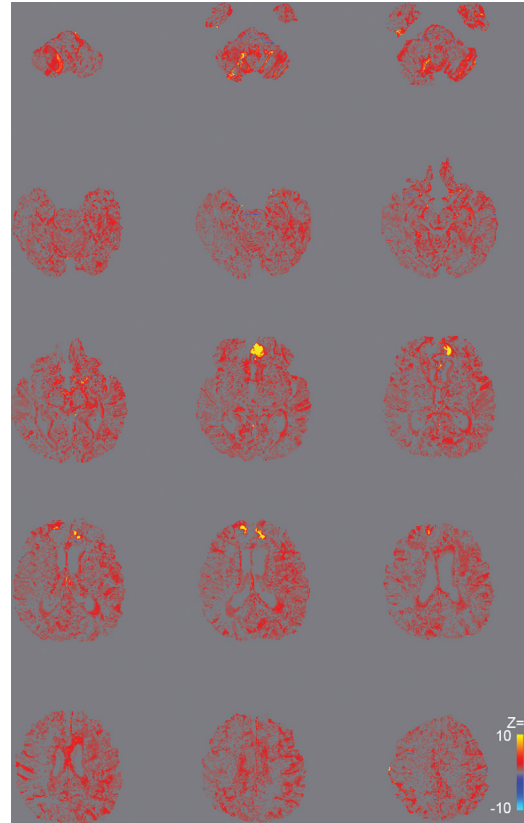
ON-LINE FIG 14. A re-analysis of the data without assumptions for the pattern of change across T1WI, ADC, and FLAIR sequences was performed on all patients in cohort 2. Unthresholded axial images in On-line Figs 14–17 are provided for patients A, B, C, and D, respectively. The results demonstrate areas that highly correlate with the model generated in cohort 1 that align with those demonstrated for the hypothesis-driven approach, but with a higher background noise.



ON-LINE FIG 15. Unthresholded axial images for patient B.



ON-LINE FIG 16. Unthresholded axial images for patient C.



ON-LINE FIG 17. Unthresholded axial images for patient D.